Direct observation of temperature dependent magnetic domain structure of the multiferroic $La_{0.66}Sr_{0.34}MnO_3/BiFeO_3$ bilayer system by XLD- and XMCD-PEEM

C. Mix, S. Finizio, G. Jakob, and M. Kläui

Institut für Physik, Johannes Gutenberg Universität Mainz, Staudingerweg 7, D-55128 Mainz, Germany

M. Buzzi and F. Nolting

Swiss Light Source, Paul Scherrer Institut, CH-5232 Villigen PSI, Switzerland

F. Kronast

Helmholtz-Zentrum-Berlin für Materialien und Energie GmbH, Albert-Einstein Straße 15, D-12489 Berlin, Germany

(Dated: March 3, 2017)

Abstract

Low-thickness $La_{0.66}Sr_{0.34}MnO_3$ (LSMO)/$BiFeO_3$ (BFO) thin film samples deposited on $SrTiO_3$ were imaged by high resolution x-ray microscopy at different temperatures. The ultra-thin thickness of the top layer allows to image both the ferromagnetic domain structure of LSMO and the multiferroic domain structure of the buried BFO layer, opening a path to a direct observation of coupling at the interface on a microscopic level. By comparing the domain size and structure of the BFO and LSMO we observed that, in contrast to LSMO single layers, LSMO/BFO multilayers show a strong temperature dependence of the ferromagnetic domain structure of the LSMO. Particularly, at 40 K, a similar domain size for BFO and LSMO is observed. This indicates a persistance of exchange coupling on the microscopic scale at a temperature where the exchange bias as determined by magnetometer measurements is vanishing.

PACS numbers: 81.15.Fg, 75.50.Pp, 77.55.Nv, 77.84.Bw, 77.80.B-, 68.37.Yz

The investigation of the ferroelectric and magnetic properties of multiferroics is a field of increasing interest [1]. Improvements in the fabrication of single crystalline Perovskite thin films led to a better understanding of the properties of multiferroics [2, 3]. $BiFeO_3$ (BFO) is one of the few room temperature multiferroics, presenting both an antiferromagnetic and a ferroelectric order [4], with a critical temperature of 1043 K for the ferroelectric polarization [5] and a Neél temperature of 643 K for the antiferromagnetic order [6], making the multiferroic properties of BFO easily accessible at room temperature. This allows one to employ the BFO for the fabrication of artificial multiferroic systems aimed at the control of the magnetization of a ferromagnetic material by means of a magneto-electric coupling. However, before one can employ this interesting material in the fabrication of multiferroic devices, a full characterization of the coupling mechanism needs to be carried out. Microscopic studies on the coupling between BFO and ferromagnetic materials such as polycrystalline CoFe have been recently carried out [7]. However, a microscopic characterization of the coupling between BFO and a ferromagnetic material such as $La_{0.66}Sr_{0.34}MnO_3$ (LSMO), presenting an epitaxial interface with the BFO, in order to gauge the influence of the interface on the coupling, are still lacking. Moreover, LSMO presents a Curie temperature above 300 K [8], thus rendering the LSMO/BFO bilayer system promising for characterization and device fabrication [9].

In this work, we report on imaging of the ferromagnetic and antiferromagnetic domain structure of the LSMO/BFO artificial multiferroic system by x-ray magnetic circular dichroism (XMCD) and x-ray linear dichroism (XLD) photoemission electron microscopy (PEEM). As the maximum information depth of x-ray PEEM is around 5-6 nm [10], an ultrathin film of LSMO (5 nm) was grown as top layer, thus allowing for the imaging of both the ferromagnetic domain structure of LSMO and the multiferroic domain structure of the 8 nm thick buried BFO layer. The subsequent comparison of the domain structures opens a path for the investigation of the exchange coupling at a microscopic scale, not possible with other more established but integrating techniques, such as superconducting quantum interference device (SQUID) magnetometry and x-ray spectroscopy. Further analyses of the coupling at temperatures, varying between room temperature (RT) and 40 K, show a strong temperature-dependent evolution of the ferromagnetic domain structure of the LSMO, not observed for LSMO thin films grown directly on $SrTiO_3$ (STO). The investigation and comparison of the domain sizes and shapes show the existence of coupling phenomena at the

microscopic scale at low temperatures.

LSMO/BFO thin film samples were fabricated by pulsed laser deposition using a Compex Pro laser at 248 nm providing 20 ns laser pulses. In this work, a spherical ultra high vacuum (UHV) chamber with an additional load-lock system is used to ensure a base pressure of $5 \cdot 10^{-8}$ mbar. The laser energy density was set to 1.2 J/cm^2 at a laser repetition rate of 5 Hz. During the deposition, substrate temperatures of 550 °C and 580°C for LSMO and BFO were used, respectively. The substrate temperature control, crucial for a correct deposition, was realized using a pyrometer camera (DIAS infrared). After depositing the BFO bottom layer at a pressure of $1.0 \cdot 10^{-2}$ mbar of oxygen, the LSMO layer was deposited at a pressure of 0.15 mbar of oxygen. To ensure full oxygen saturation, and to minimize oxygen depletion at the surface, the samples were annealed *in-situ* at a temperature of 550 °C, and at a pressure of 200 mbar of oxygen. The growth conditions for the BFO were chosen to obtain single crystalline thin films [11, 12], a Bi:Fe ratio of 1.15:1 for the ablation target, to compensate for the loss of Bismuth during deposition [11].

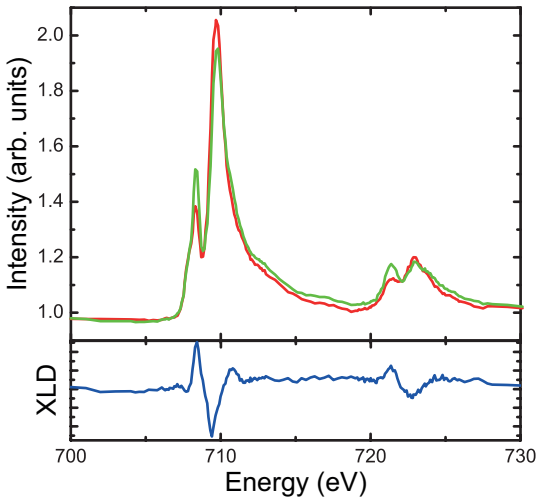

Figure 1: X-ray absorption spectra acquired at the Fe L-edge with horizontally (red) and vertically (green) polarized x-rays and the corresponding relative linear dichroism spectrum (blue).

The LSMO/BFO bilayer samples were heteroepitaxially deposited onto (001) oriented STO substrates. The deposition rates were determined by x-ray reflectometry (Phillips X'pert Pro) measurements. In this work, the BFO and LSMO layers were grown with thicknesses of 8 nm and 5 nm, respectively. By the use of a shadow mask during the growth of the LSMO layer, an area not covered by LSMO was created, enabling for the imaging of the ferroelectric domain structure of the BFO by techniques such as piezo force microscopy

(PFM). Besides allowing for PEEM imaging of both layers, these thickness levels ensure a smooth growth mode for both materials (i.e. the surfaces of both layers are atomically flat), thus avoiding the formation of a domain structure dominated by the mosaic crystallite structures that these materials present at higher thicknesses [13].

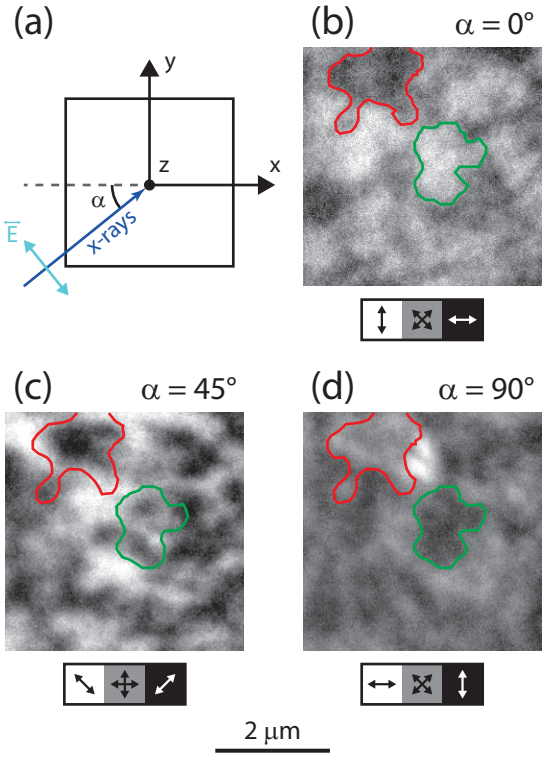

Figure 2: (a) Experimental geometry (top view), illustrating the definition of the coordinate system. The electric field of the linearly polarized x-rays lies in the xy plane of the sample, and the x-rays have an incidence angle of 16° with respect to the xy plane; (b)-(d) XLD-PEEM images of the same area showing changes in the contrast due to rotation of the analysis direction. Two domains are highlighted by green and red markings as a guide for the eye. Sub-micron domain features are also visible in the image. The grayscale bar indicates the direction of the ferroelectric/antiferromagnetic domains in the images.

The ferromagnetic domain configuration of the LSMO top layer has been imaged by XMCD-PEEM, tuning the energy of the circularly polarized x-rays to the L_3 edge of Mn (642.6 eV, corresponding to the highest dichroic contrast). The antiferromagnetic domain configuration of the BFO bottom layer has been imaged by XLD-PEEM, with the linear polarization of the incoming x-rays parallel to the surface of the sample. As can be observed in Fig. 1, where an XLD spectrum of the BFO buried layer is presented, dichroic contrast has been obtained by subtracting images taken with linearly polarized x-rays of 722.8 and 721.5 eV (L_2 edge of Fe). The imaging was carried out at the L_2 edge, as the energy difference

between the two multiplet peaks is higher than the one at the L_3 edge of Fe, allowing for the reduction of artifacts due to the limited energy resolution of the monochromating mirror. An XLD-PEEM image of the BFO buried layer taken at different rotation angles of the sample is presented in Fig. 2, showing the expected changes in the contrast with rotation of the analysis direction. This confirms that the XLD signal originates from the domain structure of the BFO. The PEEM analyses were carried out at the SIM (X11MA) beamline at the Swiss Light Source [14] and at the UE49-PGM-a beamline at BESSY II [15], both equipped with an Elmitec PEEM setup (type LEEM-III). The measurement temperatures ranged from 200 to 40 K, the lowest achievable temperature at this instrument.

For pre-characterization, the samples were investigated by PFM (Veeco Dimension D3100) to image the ferroelectric domain structure and by SQUID (Quantum Design) to determine the exchange bias effect at low temperatures. Exchange bias coupling is visible from a shift of the magnetization hysteresis after field cooling at opposite fields below the blocking temperature [9]. Fig. 3(a) shows a shift of 260 Oe for the two hysteresis loops at 3 K, which indicates the existence of an exchange bias coupling at the interface. Identical measurements were carried out at 10 K, and a shift of 100 Oe was observed. This qualitative macroscopic indication for the exchange bias was no longer detectable at 40 K, which constitutes the lowest possible temperature for PEEM analysis. In addition, Fig. 3(b) shows an image of the out-of-plane PFM phase at an area not covered by LSMO, which allows for a qualitative comparison of shape and size of the ferroelectric domains and the domains imaged by XLD-PEEM.

As shown in Fig. 4, the ferromagnetic domain structure of the top LSMO layer shows a strong variation when imaged at different temperatures. For this reason, XMCD-PEEM imaging has been carried out over a wide temperature range. At RT, no ferromagnetic contrast was observed. Only at temperatures lower than ca. 200 K, the magnetic contrast was detectable. This could be due to the low top layer thickness reducing the Curie temperature or the lower Curie temperature of the surface magnetization [16]. Fig. 4(a) shows an XMCD-PEEM image of the top LSMO layer at 200 K, illustrating a typical stripe-like domain pattern [17]. When the temperature is lowered, the formation of sub-micron domain structures is observed, as shown in Fig. 4(b)-(d). At the lowest accessible temperature, the domain structure resembles the ferroelectric domain structure of BFO imaged at an area without an LSMO top layer (Fig. 3(b)). The domain structure of the BFO, imaged with

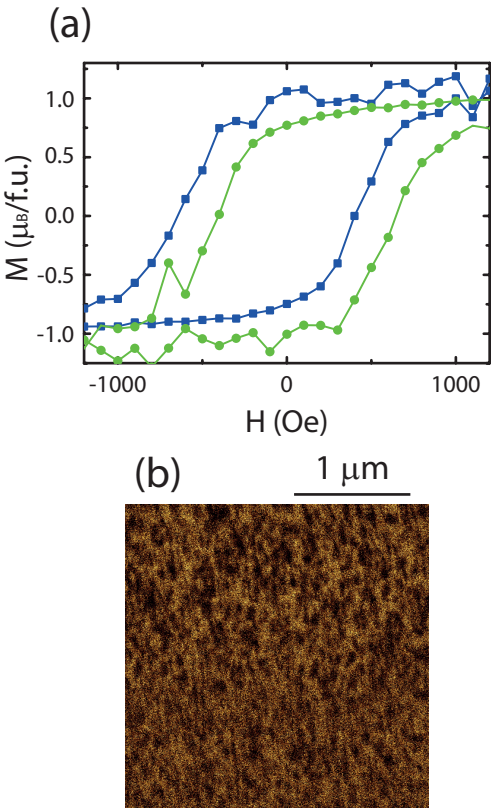

Figure 3: (a) Magnetization of a LSMO (5nm)/BFO (8 nm)/STO sample as a function of applied magnetic in-plane field. Blue and green hysteresis loops were measured at 3 K after field cooling from above the Curie temperature with a magnetic field of ± 500 Oe applied, respectively. (b) Image of the out-of-plane PFM phase of the same sample in an area not covered by LSMO showing domains of sub-micron size.

XLD-PEEM, did not show any modifications when lowering the temperature from RT to 40 K. Moreover, in order to investigate possible magnetoelectric or exchange coupling of the domain structure of LSMO and BFO at the microscopic scale, the same area of the bilayered system has been imaged by XLD- and XMCD-PEEM. In Fig. 5, XLD- and XMCD-PEEM imaging was employed to determine and compare at the same position the antiferromagnetic and ferromagnetic domain structure of the buried BFO layer and of the top LSMO layer, respectively. As can be observed in Fig. 5, the structure and size of the domains is comparable. However, despite the similarities, no direct matching of the shape and direction of the domains was observed. As already shown by P. Yu et al. [18], the investigation of the exchange coupling of the LSMO/BFO bilayer system is limited to very low temperatures (T$\leq$100 K). The exchange bias analyses shown in Fig. 3(a) have already indicated that a macroscopic exchange coupling is observable only at temperatures lower than the

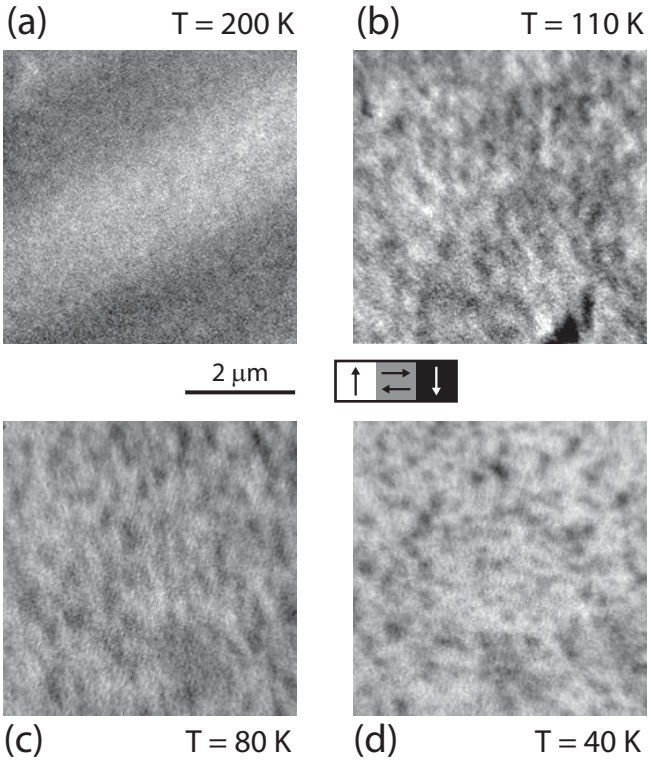

Figure 4: XMCD-PEEM images of the LSMO top layer of a LSMO (5nm)/BFO (8 nm)/STO sample taken at different temperatures. Images (b), (c) and (d) are taken at exactly the same position, image (a) is taken at another position of the same area. The grayscale bar indicates the direction of the magnetic contrast in the images.

lowest accessible temperature for PEEM imaging. From these results we observe that the ferromagnetic LSMO domain structure at temperatures of 200 K and above is not affected by exchange coupling to the BFO layer. As the temperature is reduced, the similarities in size and shape of LSMO and BFO domains especially at the lowest accessible temperatures indicate coupling effects at the interface of the two materials.

In conclusion, samples of the LSMO/BFO artificial multiferroic system were prepared by pulsed laser deposition and subsequently analyzed by x-ray PEEM imaging. The ultrathin thickness of the top LSMO layer allowed for the imaging of both the ferromagnetic and antiferromagnetic domain structure of LSMO and BFO, respectively. This has shown to be a promising approach for the investigation of the multiferroic coupling in a full oxide bilayer system.

The ferromagnetic domain structure of the LSMO was imaged in a temperature range between RT and 40 K, and the domain structure of LSMO at low temperatures resembles the antiferromagnetic BFO in size and shape, although a direct match of the domain shape

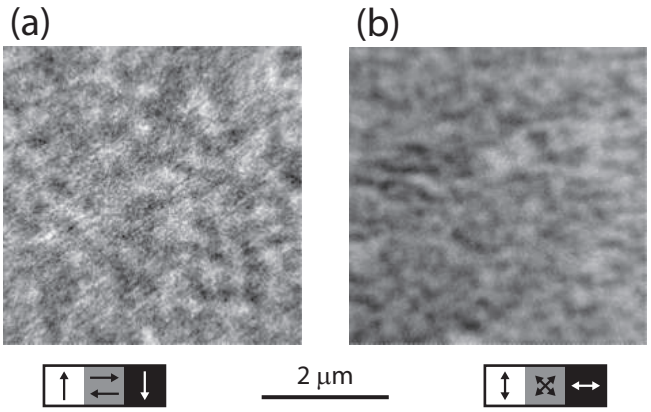

Figure 5: (a) XMCD-PEEM image of the LSMO top layer. (b) XLD-PEEM image at the same position of the BFO buried layer. Both images were acquired at 40 K. The grayscale bars indicate the different interpretation of the contrast in the two images.

and direction was not observed. As this temperature-dependent change in the domain structure of the LSMO is not present for LSMO layers of this thickness grown on STO, the changes result from the growth on BFO. Thus, the direct imaging by PEEM with high spatial resolution allowed to reveal coupling effects even in absence of a macroscopic exchange bias effect and has shown to be a promising approach for the investigation of the multiferroic coupling in a full oxide bilayer system. In future, the artificial multiferroic bilayer system presented here will allow a poling of the ferroelectric polarisation. Combined with a microstructuring of the bilayer samples this will yield defined magnetic structures and will simplify the observation and interpretation of multiferroic coupling at the interface.

Part of this work has been carried out at the Swiss Light Source, Paul Scherrer Institut, Villigen, Switzerland and at the Helmholtz-Zentrum-Berlin, Germany. The authors further acknowledge the financial support from the EU 7th Framework Project IFOX (NMP3-LA-2010 246102), the Stiftung Rheinland-Pfalz für Innovation (grant 961-386261/944), the Swiss National Science Foundation, the Graduate School of Excellence 'Materials Science in Mainz' (GSC 266), and the Deutsche Forschungsgemeinschaft (DFG).

---

[1] N.A. Spaldin, and M. Fiebig, Science **309**, 391 (2005)

[2] S. Ohashi *et al.*, Rev. Sci. Instr. **70**, 187 (1999)

[3] D. G. Schlom *et al.*, Mater. Sci. Eng. B **87**, 282 (2001)

[4] Y.-H. Chu *et al.*, Materials Today **10**, 10 (2007)

[5] J.R. Teague, R. Gerson, and W.J. James, Sol. St. Com. **8**, 1073 (1970).

[6] S.V. Kiselev, R.P. Ozerov, and G.S. Zhdanov, Sov. Phys. Dokl. **7**, 742 (1963).

[7] M. Trassin *et al.*, Phys. Rev. B **87**, 134426 (2013)

[8] G.H. Honer, and J.H. van Santen, Physica **16**, 337 (1950)

[9] S. M. Wu *et al.*, Nature Mater. **9**, 756 (2010)

[10] G. Schönhense, J. Phys.: Condens. Matter **11**, 9517 (1999).

[11] H. Béa *et al.*, Appl. Phys. Lett. **87**, 072508 (2005).

[12] C. Mix, and G. Jakob, J. Appl. Phys. **113**, 17D907 (2013).

[13] H. Boschker *et al.*, J. Phys. D: Appl. Phys. **44**, 205001 (2011).

[14] U. Flechsig *et al.*, AIP Conf. Proc. **1234**, 319 (2010).

[15] F. Kronast *et al.*, Surf. and Int. Analysis **42**, 1532 (2010).

[16] R. Reeve *et al.*, Appl. Phys. Lett. **102**, 122407 (2013)

[17] J. Rhensius *et al.*, Appl. Phys. Lett. **99**, 062508 (2011).

[18] P. Yu, and R. Ramesh, Materials Today **15**, 7 (2012)